New Journal of Physics

The open access journal at the forefront of physics

PAPER

OPEN ACCESS

Eleven competing phases in the Heisenberg-Gamma ($J\Gamma$) ladder

Sebastien J Avakian and Erik S Sørensen[*] ![ORCID]

Department of Physics & Astronomy, McMaster University, Hamilton, ON L8S 4M1, Canada
[*] Author to whom any correspondence should be addressed.

E-mail: sorensen@mcmaster.ca

Abstract

The spin-orbit generated Γ interaction is known to induce strong frustration and to be significant in realistic models of materials. To gain an understanding of the possible phases that can arise from this interaction, it is of considerable interest to focus on a limited part of parameter space in a quasi one-dimensional model where high precision numerical results can be obtained. Here we study the Heisenberg–Gamma ($J\Gamma$) ladder, determining the complete zero temperature phase diagram by analyzing the entanglement spectrum (ES) and energy susceptibility. A total of 11 different phases can be identified, among them the well known rung-singlet (RS) phase and 5 other phases, FM, FM-Z, FM-XY, AF and AF-Z, with conventional long-range magnetic order. The 3 ferromagnetic phases, FM, FM-Z and FM-XY simultaneously have non-zero scalar chirality. Two other phases, the antiferromagnetic Gamma (AΓ) and ferromagnetic Gamma (FΓ) phases, have previously been observed in the Kitaev–Gamma ladder, demonstrating that the AΓ-phase is a symmetry protected topological phase (SPT) protected by TR$\times\mathcal{R}_b$ symmetry, the product of time-reversal (TR) and π rotation around the b-axis ($\mathcal{R}_b$), while the FΓ-phase is related to the RS phase through a local unitary transformation. The 3 remaining phases, Υ, Ω and δ show no conventional order, a doubling of the ES and for the Υ and Ω-phases a gap is clearly present. The δ-phase has a significantly smaller gap and displays incommensurate correlations, with a peak in the static structure factor, $S(k)$ continuously shifting from $k/\pi = 2/3$ to $k = \pi$. In the Ω-phase we find pronounced edge-states consistent with a SPT phase protected by the same TR$\times\mathcal{R}_b$ symmetry as the AΓ-phase. The precise nature of the Υ and δ-phases is less clear.

1. Introduction

Often when modelling magnetic materials, the interaction terms are assumed not to depend on the direction of the bond, in the sense that terms that can only be distinguished by their spatial orientation are taken to be equivalent. Significant interest in models where this is not the case and interactions depend on the direction of bonds, have arisen with Kitaev's exact solutions for the ground-state of a simple local Hamiltonian with bond-directional interactions on a honeycomb lattice, the Kitaev Honeycomb model (KHM) [1]. Bond-directional interactions have previously been considered in the wider context of quantum compass (Kugel–Khomskii) models [2–5], however, for the KHM a spin liquid ground-states can rigorously be demonstrated [1]. The bond-directional Kitaev interaction (K) in the KHM is of the Ising type and can be realized in real materials, as demonstrated by Chaloupka *et al* [6]. This has established the class of Kitaev materials [7–11] that are currently being intensely studied. Among the most promising candidate materials is α-RuCl$_3$ [12–14], a material with two-dimensional honeycomb layers. For α-RuCl$_3$ there is growing consensus [8, 9, 15, 16] that the Kitaev interaction is ferromagnetic $K < 0$, however, other interactions are clearly also present [17, 18] with the Γ-interaction the largest [19, 20]. On a given a bond with a Kitaev interaction of the form $KS^\gamma S^\gamma$, the Γ-interaction takes the form $\Gamma(S^\alpha S^\beta + S^\beta S^\alpha)$ and it is estimated [8, 9, 15, 16] that $\Gamma > 0$ in α-RuCl$_3$. Interaction terms of the usual Heisenberg form with strength J are also believed to be non-negligible, but smaller than the Γ-interaction. Several other interaction terms, such as Γ', J_2 and J_3 are sometimes also taken into considerations, but they are believed to be even smaller in magnitude for

α-RuCl$_3$, and we do not discuss them here even though they might crucially influence the phase-diagram due to the very high degree of frustration. The phase diagram of α-RuCl$_3$ is of significant current interest due to the experimental observation a magnetically disordered phase under an applied magnetic field [13, 14, 21] which has been interpreted as a spin liquid phase [22, 23]. The precise nature of this phase is debated [24–27] and a full understanding of the complete phase diagram is lacking. Furthermore, it is clear that the complete phase-diagram of the K–J–Γ model of α-RuCl$_3$ in a magnetic field is very complex and extremely challenging to determine precisely [17, 28–30]. It is therefore very valuable to study the phase diagram of low dimensional versions of this model in a highly restricted part of parameter space where almost exact results can be obtained from state of the art numerical calculations, and here we focus on the Heisenberg Gamma ($J\Gamma$) in a ladder geometry.

While the ladder is a highly restrictive geometry, it can still lead to important insights into the possible phases of the full two-dimensional models, and it includes crucial interactions not present in a purely one-dimensional model. We also note that classes of ladder materials exists that have been shown to closely model the ladder geometry [31, 32], so called spin-ladder materials, and one might hope that it will be possible to find similar materials with bond-directional interactions. The ladder geometry is also very attractive since almost exact results can be obtained for extremely large systems or directly in the thermodynamic limit, in stark contrast to the two-dimensional lattice where exact diagonalization results are limited to very small sizes [17, 33]. Multi-leg models have been studied [34, 35] but systematic studies are challenging. Kitaev's [1] solutions of the honeycomb model can be extended to include the ladder [36] but is not applicable when $J \neq 0$ or $\Gamma \neq 0$. The Kitaev–Heisenberg model in a ladder geometry has been studied using numerical techniques [37–39] finding 6 distinct phases at zero field as the ratio J/K is varied, in remarkable good agreement with exact diagonalization results for the honeycomb lattice [40]. Likewise, the Kitaev–Gamma ladder has also been investigated [41–43], and in this case 8 distinct phases can be identified in zero field versus Γ/K. The Heisenberg–Gamma ($J\Gamma$) ladder is relatively less explored, and from the exact diagonalization results in [17] the line in the phase diagram of the honeycomb lattice corresponding to the $J\Gamma$-model appear to only cross a modest number of phases. Here we show that the phase diagram of the $J\Gamma$-ladder is significant richer, with a total of 11 distinct phases appearing in zero field. In addition to 5 phases, FM, FM-Z, FM-XY, AF and AF-Z, with conventional long-range magnetic order we observe three previously discussed phases, the RS, FΓ and AΓ-phases, where the RS and FΓ-phases are related by a local unitary transformation [44]. However, we also find three new potential symmetry protected topological phase (SPT) phases, that we denote Υ, Ω and δ. These 2 phases show no conventional order, a doubling of the entanglement spectrum ES and for the Υ and Ω-phases a relatively clear gap, consistent with SPT behavior.

SPT phases in gapped one-dimensional spin systems can be classified using a projective symmetry analysis [45–47]. Usually the site symmetries given by $D_2 = \{E, R_x, R_y, R_z\}$ is considered where $R_x(R_y, R_z)$ is a π rotation about the $x(y, z)$ axis. The projective analysis can be extended to ladders [48–53] where the additional symmetry σ, arising from interchanging the legs of the ladder is also included, and the group $D_2 \times \sigma$ is considered. It is important to note that a local unitary transformation, U_6 exists [44], that maps the Kitaev–Gamma ($K\Gamma$) ladder to a model with $D_2 \times \sigma$ site symmetry. While σ is not a good symmetry for the Kitaev–Heisenbergv (KJ) ladder, it does have the D_2 symmetry. However, neither D_2 nor σ is a good symmetry for the $J\Gamma$-ladder and the U_6 transformation is not useful. Instead, the σ symmetry is replaced by a non-symmorphic symmetry, involving both reflection and translation. In the following, we therefore mainly focus on the time-reversal (TR) symmetry present in the $J\Gamma$-ladder in zero field. It can therefore be argued that the effect of the Γ-interaction is particularly relevant for the $J\Gamma$-ladder that is our focus here, due to the significant reduction in the symmetry.

The outline of the paper is as follows. In section 2, we introduce the $J\Gamma$-ladder, the geometry and the parametrization. The bulk of our results are obtained using DMRG and iDMRG techniques, and in section 3 we discuss the specifics of our numerical methods along with the conventions used. In section 4 we present our main results for the phase-diagram of the $J\Gamma$-ladder, demonstrating the presence of 11 distinct phases. In section 5 the magnetically ordered phases are discussed along with the chiral ordering we observe in the ferromagnetic phases. The RS, AΓ and FΓ-phases are discussed in section 6. Finally, the three new potential SPT phases, Υ, Ω and δ and their classification are discussed in section 7 where we also discuss the projective symmetry analysis of the TR symmetry.

2. The $J\Gamma$-ladder

Our focus is on the two leg ladder derived from the honeycomb lattice. To get as faithful a representation of the honeycomb lattice as possible, we consider a small strip of the honeycomb material, shown in figure 1(c), and create a two leg ladder by ensuring that the bonds that are cut perpendicular to the length of the ladder are paired together, effectively imposing periodic boundary conditions (PBC) in the perpendicular direction.
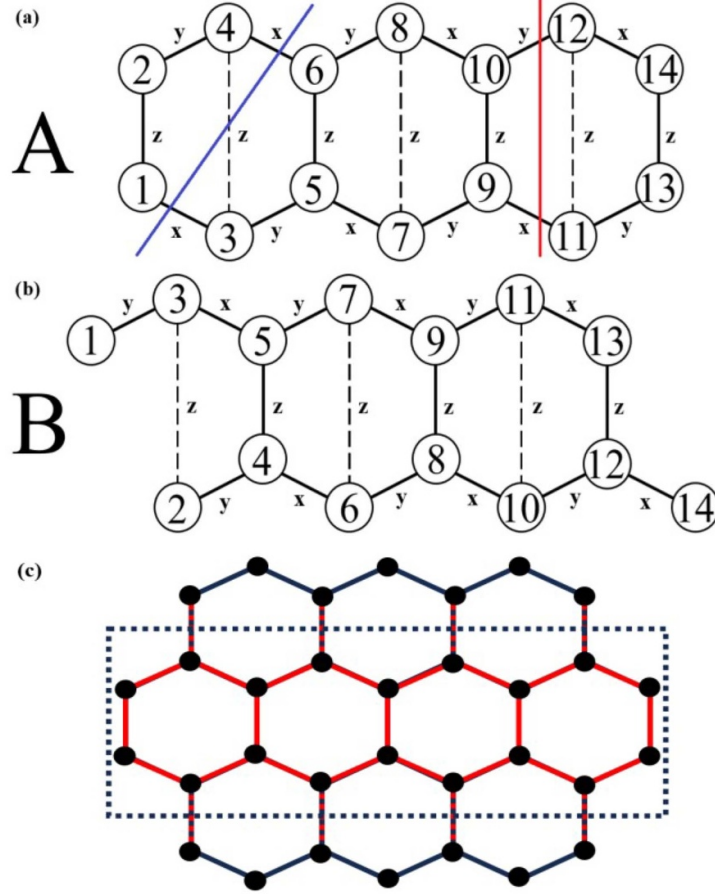
Figure 1. The two clusters of the two leg $J\Gamma$-ladder with alternating x and y bonds along the legs of the ladder, connected by z bonds along the rungs. Here the x, y and z refers to the variation in the Γ-interaction. The dashed lines indicate z bonds arising from imposing periodic boundary conditions in the perpendicular direction. (a) Cluster A formed from a regular ladder with the red line indicating a bond cut and the blue line a rung cut, relevant for forming the reduced density matrix. (b) Cluster B formed from cutting the rungs from cluster. (c) Geometry of the honeycomb ladder extracted from the full two dimensional honeycomb lattice. The ladder is formed by cutting along the dashed rectangle and pairing the dashed vertical red bonds with one another, mimicking periodic boundary conditions.

This is illustrated in figure 1 where the dashed bonds arise due to the PBC. We assume these interactions to be of the same strength as the direct coupling between the legs, shown as the solid rungs in figure 1. On each bond of the ladder, we introduce an isotropic Heisenberg interaction of strength J. The second interaction is the Γ-interaction, an asymmetric exchange interaction that crucially varies between bonds and is not the same for every bond. The corresponding Hamiltonian is then

$$H = \sum_{\langle i,j \rangle} J\mathbf{S}_i \cdot \mathbf{S}_j + \sum_{\langle i,j \rangle_\gamma} \Gamma \left(S_i^\alpha S_j^\beta + S_i^\beta S_j^\alpha \right), \tag{1}$$

where $\langle i,j \rangle_\gamma$ denotes the nearest neighbor bond of type γ. The possible kinds of bonds are $\gamma = x, y, z$ labeling the possible values of (α, β) as (y, z), (x, z), and (x, y) respectively. In other words, γ labels the missing spin component exchange present in $S_i^\alpha S_j^\beta$.

2.1. Clusters and boundaries

The J-Γ ladder, equation (1), comprises alternating x and y bonds along the both legs, connected by z bonds along the rungs. The unit cell of the ladder then consists of 4 sites, as shown in figures 1(a) and (b). When discussing properties of the model derived from the reduced density matrix of a bipartition of the lattice, it is important to take into account if the partition cuts a rung or only the legs of the ladder. This is illustrated by the blue and red lines in figure 1(a) showing a rung (blue) and bond (red) cut respectively. When considering edge-states that may appear in SPT phases, we shall consider finite open segments of the ladder, and it is then crucial to consider how the open boundary conditions (OBC) are imposed. For the ladder, we consider the two possibilities shown in figures 1(a) and (b). We refer to the first (regular) cluster as A and the second (rung cut) cluster as B. The degeneracy of the ground-state in a SPT phase strongly depends on whether open

or PBCs are applied, however, as we shall see in the following, the degeneracy of the ground-state can also depend on whether cluster A or B is used.

2.2. Parametrization and connections to known models

The overall scale for the coupling constants, J and Γ are not relevant, and it is therefore convenient to parameterize them in the following way

$$J = \sin(\phi), \; \Gamma = \cos(\phi). \tag{2}$$

The phase space of the model can then be parameterized by the angle ϕ. Some points in the phase-diagram correspond to models that have previously been studied in detail. At $\phi = \pi/2$ the $J\Gamma$-ladder is simply the antiferromagnetic (AF) Heisenberg ladder for which it has been established that the ground-state is a rung-singlet (RS) state with a sizable gap [31, 54, 55]. Similarly, at $\phi = 3\pi/2$ we find the well known ferromagnetic Heisenberg ladder that we expect to show gapless spin wave excitations.

The model with a pure antiferromagnetic Γ-interactions occurring at $\phi = 0$, has previously been studied in detail [41–43] and it is known that the model is in a SPT phase with a gap. In addition, a string order parameter has been found [43]. Interestingly, the same antiferromagnetic Γ-model on the two-dimensional honeycomb lattice is believed to exhibit a gapless spin liquid phase [56] although other scenarios have been discussed [28, 35, 57].

Finally, at $\phi = \pi$ we find the ferromagnetic Γ-ladder. If we at this point apply the local unitary U_6 transformation [44], the FΓ-ladder can be mapped to an antiferromagnetic spin ladder with nearest neighbor interactions only of the type $S_i^x S_j^x$, $S_i^y S_j^y$ and $S_i^z S_j^z$. Such an AF spin ladder has been shown [42] to be in the same phase as the isotropic AF spin ladder with isotropic $\mathbf{S}_i \cdot \mathbf{S}_j$ interactions on each bond which is known to be in the RS phase, as discussed above. The FΓ-phase, of which the $\phi = \pi$ is part, can therefore also be labelled RS_{U_6} since it is related to the RS-phase through the local unitary U_6 transformation.

3. Methods

The main tool used in this analysis is the finite density matrix renormalization group (DMRG) [58–63] and its infinite sized version, the infinite DMRG (iDMRG) [64]. The finite size version will be used to obtain the ground state and the next 4 excited states with OBC and periodic boundary conditions (PBC). For the OBC, we mainly use a maximal bond dimension $D = 1000$ and a precision of $\epsilon = 10^{-13}$, while with PBC we typically use $D = 1200$ and $\epsilon = 10^{-11}$. To obtain the ground state in the thermodynamic limit, produce the phase diagram, and calculate the bulk correlation functions, we use iDMRG with $D = 1000$ and $\epsilon = 10^{-11}$. In order to ensure that we detect all possible phases, the maximum resolution we use is $\Delta\phi/\pi = 0.001$.

To detect the quantum critical points (QCP), we use two measures of the ground state wavefunction, the first being the susceptibility of the ground state energy per spin e_0 with respect to ϕ

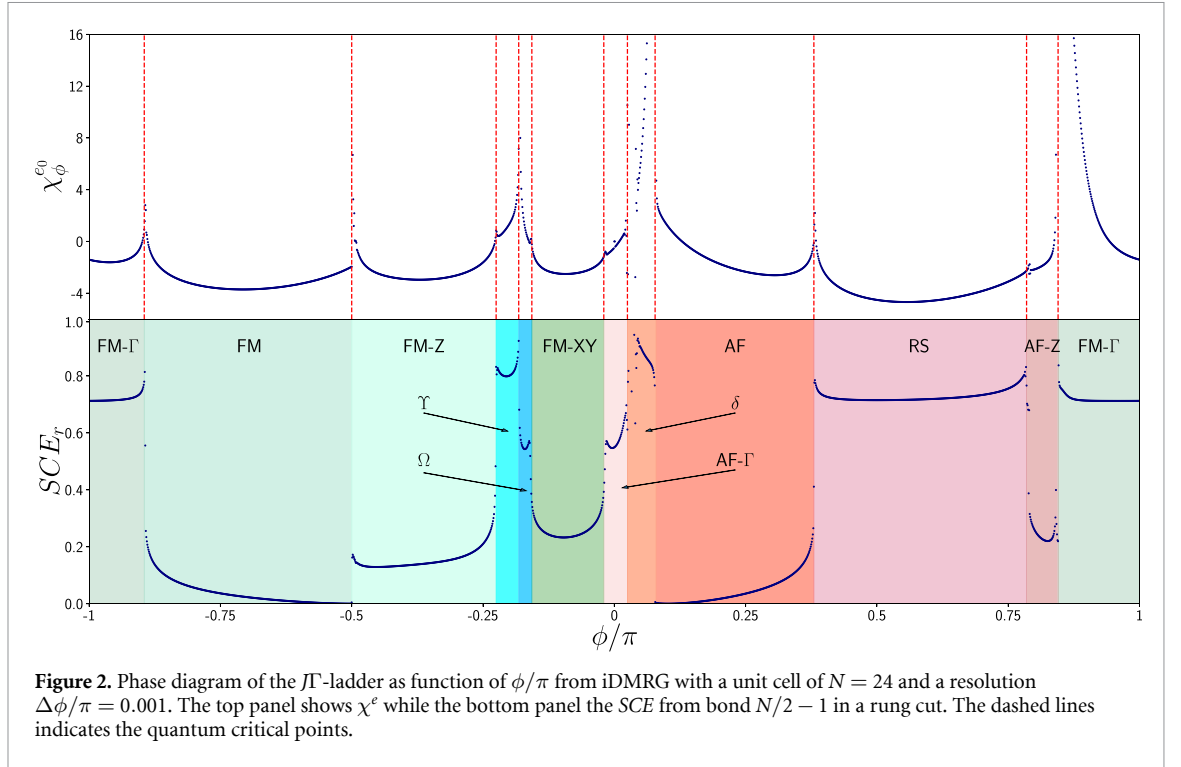$$\chi_\phi^e = -\frac{\partial^2 e_0}{\partial \phi^2}. \tag{3}$$

In finite systems, at a QCP, χ^e has been shown to scale as [65–67]

$$\chi^e \sim N^{2/\nu-d-z}. \tag{4}$$

Here ν and z are the correlation and dynamical critical exponents and d is the dimension. Hence, only when $2/\nu > d + z$ will χ^e diverge. If we assume that $z = 1$ and with $d = 1$ we find that $\nu < 1$ as a condition for a divergence to occur. In addition, the divergence might be very narrow and could be missed if $\Delta\phi$ is not sufficiently small. In principle, when studying systems in the thermodynamic limit with iDMRG, χ^e should be infinite at the QCP but the finite resolution in ϕ will instead show a very sharp spike instead. It is therefore very useful to have a complementary way of determining the phase diagram, and for quasi one-dimensional models this can be obtained from the entanglement spectrum. If we cut the ladder across the bond n and form the reduced density matrix ρ_n the ES can be obtained from the eigenvalues λ_i of ρ_n. The eigenvalues change slowly away from a QCP but rapidly near a QCP. Sometimes the so-called Schmidt gap [68–71], the difference between the two largest eigenvalues, is studied, but here we focus on just the leading eigenvalue λ_1 which defines the single copy entanglement [72]

$$SCE = -\ln(\lambda_1). \tag{5}$$

When the ground state is in a product state, we must have that $\lambda_1 = 1$ and $\lambda_n = 0, \forall n > 1$ implying that SCE = 0. On the other hand, if our system is not in a product state, $\lambda_1 < 1$, we must have SCE > 0. In the

Figure 2. Phase diagram of the $J\Gamma$-ladder as function of ϕ/π from iDMRG with a unit cell of $N = 24$ and a resolution $\Delta\phi/\pi = 0.001$. The top panel shows χ^e while the bottom panel the *SCE* from bond $N/2 - 1$ in a rung cut. The dashed lines indicates the quantum critical points.

ladder geometry, the only two unique bipartitions are made by either cutting through two leg bonds or through two leg bonds and a rung, as shown in i figure 1(a). As previously outlined, we shall refer to this as a 'bond' cut and a 'rung' cut, respectively. While either cut can be used for our purposes, we mainly use the rung cut, the blue line in figure 1(a), when studying the SCE.

In order to characterize the magnetic ordering of the phases, we study the spin correlation functions $\langle S_i^\alpha S_{i+n}^\alpha \rangle$ as well as the on-site magnetization $\langle S_i^\alpha \rangle$. In addition, we also study the scalar chirality. For any 3 spins $\mathbf{S} = \sigma/2$ at sites i, j and k the scalar chirality is defined as follows,

$$\kappa = \langle \sigma_i \cdot (\sigma_j \times \sigma_k) \rangle. \tag{6}$$

From this definition it seems likely that a non-zero κ will be accompanied by more conventional magnetic ordering and in section 5 we discuss the chiral ordering in more detail.

4. Phase diagram

Our main results for the phase diagram are shown in figure 2 where we show iDMRG results for χ^e in the top panel along with results for SCE in the bottom panel. The QCP are indicated by the dashed vertical lines. An astonishingly large number of phases is observed, 11 in total. From left to right we label these phases as, FΓ, FM, FM-Z, Υ, Ω, FM-XY, AΓ, δ, AF, RS and AF-Z. While most of these phases show some type of magnetic ordering, the FΓ, Υ, Ω, AΓ, δ and RS phases do not. We discuss all phases in further detail in the subsequent sections. At most of the QCP we find complete agreement between the divergence in χ^e and sharp features in the SCE. One exception is the FM-XY to AΓ transition which do not show a clear divergence in χ^e, on the other hand, it is clearly visible in the SCE. This is consistent with a value of the correlation length exponent $\nu > 1$ at this transition. A similar observation can be made about the RS to AF-Z transition. A summary of the results from figure 2 can be found in table 1 where the critical values of ϕ are listed for all phases along with their characteristics.

4.1. Degeneracies

A characteristic feature of SPT phases is that edge-states appear under OBC. A well-known example is the $S = 1$ spin chain, where $S = 1/2$ edge-states appear [73–75] above a four-fold degenerate ground-state with OBC. Another characteristic is a degeneracy of all eigenvalues in the entanglement spectrum [45, 46, 76, 76, 77]. Such a degeneracy is necessary for non-trivial transformations under the projective symmetry, as we discuss further in section 7. For the determination of the ground-state degeneracy with OBC it is crucial to distinguish between the two different clusters from figures 1(a) and (b) and we therefore refer to the resulting ground-state degeneracies as $d_{gs}^{\mathrm{OBC}_A}$ and $d_{gs}^{\mathrm{OBC}_B}$. For the entanglement spectrum, which we obtain from

Table 1. Summary of the main features of all phases of the $J\Gamma$-ladder. The phase symbol and the critical values of ϕ/π for which the phase exists are listed, as well as the magnetic ordering. The last column indicates the presence of an energy gap in the spectrum in the thermodynamic limit.

Phase	ϕ_c/π	Magnetic ordering	Energy gap
$A\Gamma$	1.983–0.025	None	Yes
δ	0.025–0.077 693	None	Possibly Gapless
AF	0.077 693–0.380	AFM	Yes
RS	0.380–0.790	RS	Yes
AF-Z	0.790–0.840	AFM-Z	Yes
$F\Gamma$	0.840–1.110	None	Yes
FM	1.110–1.500	FM	Yes
FM-Z	1.500–1.775	FM-Z	Yes
Υ	1.775–1.820	None	Yes
Ω	1.820–1.840	None	Yes
FM-XY	1.840–1.983	FM-XY	Yes

Table 2. Summary of the main features of the potential SPT phases of the $J\Gamma$-ladder. The d_{rung} and d_{bond} are the degeneracies in the spectrum of the reduced density matrix formed on cluster A or B respectively. The $d_{gs}^{\text{OBC}_A}$, $d_{gs}^{\text{OBC}_B}$, and d_{gs}^{PBC} are the ground state degeneracies in open or periodic boundary conditions with OBC$_A$ and OBC$_B$ referring to cluster A and B respectively. $\mathcal{O}_{\text{TR}}^A$ and $\mathcal{O}_{\text{TR}}^B$ are the projective phase factors under TR (see section 7.4).

Phase	d_{rung}	d_{leg}	$d_{gs}^{\text{OBC}_A}$	$d_{gs}^{\text{OBC}_B}$	d_{gs}^{PBC}	$\mathcal{O}_{\text{TR}}^A$	$\mathcal{O}_{\text{TR}}^B$
$A\Gamma$	1	2	4	1	1	-1	1
δ	2	1	1	4	1	1	-1
Υ	2	1	1	4	1	1	-1
Ω	1	2	4	1	1	-1	1

iDMRG calculations, it is important to distinguish between the rung cut and bond cut discussed above and shown as the blue and red line in figure 1(a). Our results for these degeneracies for all the potential SPT phases are listed in table 2. We find in all cases a 4-fold degeneracy of the ground-state using A or B cluster. If the degeneracy is on the $A(B)$ cluster, the ground-state on the $B(A)$ cluster is non-degenerate. Furthermore, if the 4-fold degeneracy is present on the $A(B)$ cluster, the ES show degeneracy on the bond cut (rung cut) and no degeneracy on the alternate cut. For completeness, we also list the degeneracy under PBC in table 2. These observations are consistent with the presence of SPT phases. Of these 5 phases, the $A\Gamma$ and $F\Gamma$-phases have been studied elsewhere [41–43] but before analyzing the remaining 3 potential SPT phases, Υ, Ω and δ, we turn to a discussion of the magnetically ordered phases.

5. Magnetically ordered phases
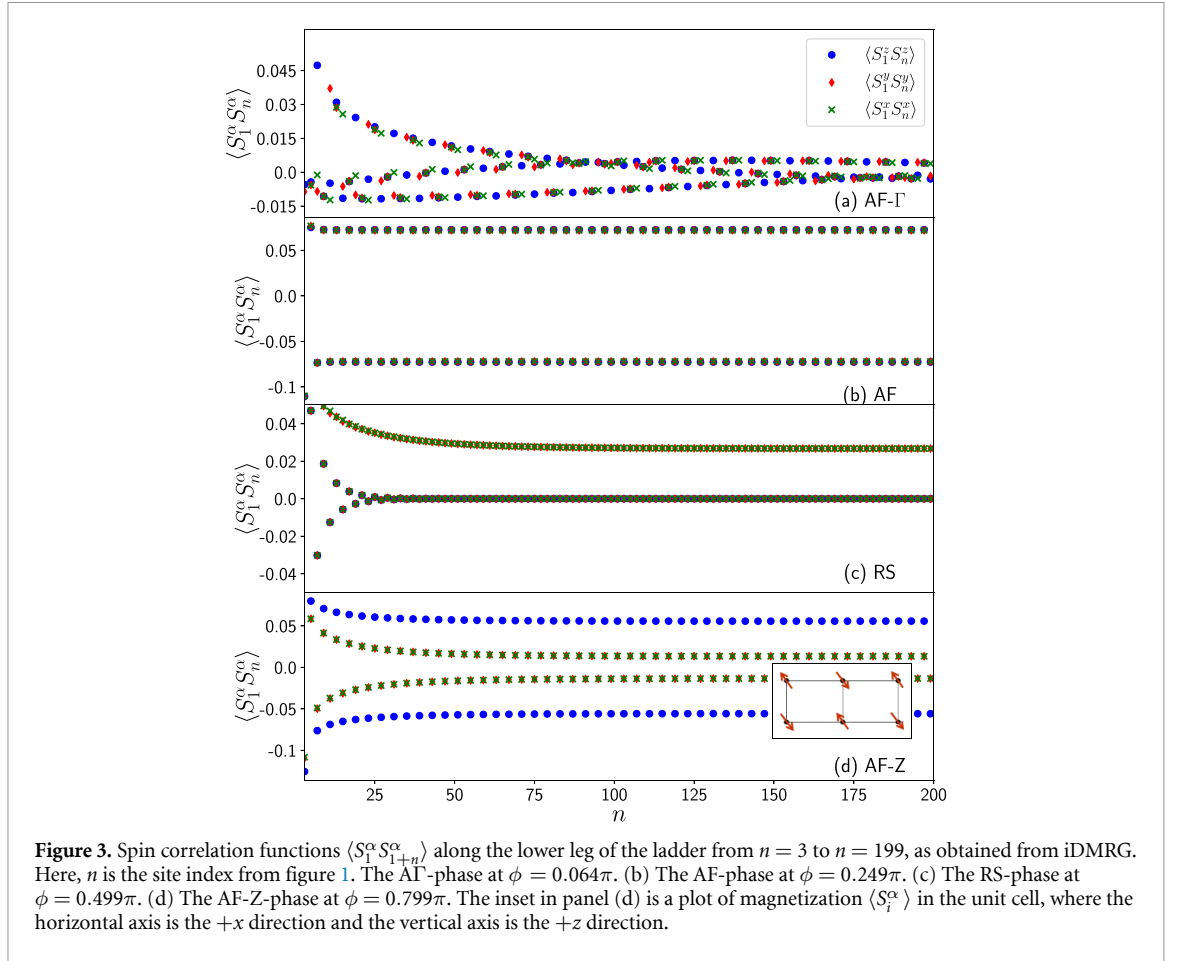
5.1. AF phases
There are two phases with clear long-range AF magnetic ordering, the AF and AF-Z-phases. In figures 3(b) and (c) we show results for the spin correlations for each phase.

- AF-phase: For $\phi/\pi \in (0.077\,693, 0.380)$, we have the AF-phase. As can be seen in figure 3(b) the spin correlations are clearly long-range and isotropic between the *x*, *y* and *z* components. The Γ-term is non-zero throughout the AF-phase, and contrary to what one might expect, the AF-phase is not gapped. In fact, as we discuss in section 7, the correlation length in this phase is rather short, indicating the presence of a well-defined gap.
- AF-Z-phase: For $\phi/\pi \in (0.79, 0.84)$, the spin correlations look similar to those of the AF phase and are again long-range. However, in this phase the $S_1^z S_n^z$ correlations are larger than the $S_1^x S_n^x$ and $S_1^y S_n^y$ correlations, which are equal, as can be seen from our iDMRG results shown in figure 3(d) and a sketch of the ordering is shown the inset. We denote this phase the AF-Z-phase. The correlation length is finite, indicating a well-defined gap.

5.2. FM phases and chiral ordering
Three of the phases, FM, FM-Z and FM-XY, have long-range ferromagnetic correlations, as can be seen from the results for the spin correlation functions $\langle S_1^\alpha S_{1+n}^\alpha \rangle$ shown in figure 4.

- FM-phase: For $\phi/\pi \in (1.110, 1.500)$ the spin correlations shown in figure 4(b) show clear long-range ferromagnetic order. Furthermore, all three spin correlation functions appear identical and the phase can be

Figure 3. Spin correlation functions $\langle S_1^\alpha S_{1+n}^\alpha \rangle$ along the lower leg of the ladder from $n = 3$ to $n = 199$, as obtained from iDMRG. Here, n is the site index from figure 1. The AΓ-phase at $\phi = 0.064\pi$. (b) The AF-phase at $\phi = 0.249\pi$. (c) The RS-phase at $\phi = 0.499\pi$. (d) The AF-Z-phase at $\phi = 0.799\pi$. The inset in panel (d) is a plot of magnetization $\langle S_i^\alpha \rangle$ in the unit cell, where the horizontal axis is the $+x$ direction and the vertical axis is the $+z$ direction.

identified as an isotropic ferromagnetic phase. As was the case for the AF phases, the FM-phase is gapped, a fact that we infer from the presence of a relatively short correlation length.

- FM-Z-phase: Neighboring the FM-phase is the FM-Z-phase for $\phi/\pi \in (1.500, 1.775)$, This phase is similar to the FM-phase but in the FM-Z-phase the $S_1^z S_n^z$ correlations are larger than the $S_1^x S_n^x$ and $S_1^y S_n^y$, which are equal, as illustrated in figure 4(c). A sketch of the ordering is shown in the inset in figure 4(c). We therefore denote the phase FM-Z. Similar to the FM-phase, the FM-Z-phase has a finite correlation length and a gap.

- FM-XY-phase: The last ferromagnetic phase is the FM-XY-phase appearing for $\phi/\pi \in (1.840, 1.983)$ where we show results in figure 4(d). Depending on which leg of the ladder is analyzed, the spin correlations have either the $S_1^x S_n^x$ or $S_1^y S_n^y$ correlation marginally larger than the other at small n and then finally equalling each other at larger n. Along both legs, the $S_1^z S_n^z$ correlations are smaller than the other two and non-zero. However, along one leg of the ladder the local magnetization is aligned in the opposite direction of the other leg. A sketch of the ordering is shown in the inset in figure 4(d). We denote the phase FM-XY. Correlations in the FM-XY-phase are characterized by a sizable, but still finite correlation length and therefore a finite gap.

It is interesting to note that precisely at $\phi/\pi = 3/2$ the $J\Gamma$-ladder is simply a ferromagnetic Heisenberg ladder, since $\Gamma = 0$. For the FM Heisenberg ladder we would expect gapless spin-wave excitations and an infinite correlation length. This is indeed the case, since for the $J\Gamma$-ladder this point corresponds to the transition between the FM and FM-Z phases. However, both the FM and FM-Z-phases are gapped, demonstrating the strong effect of the Γ-interaction.

From the structure of the Γ term, it is plausible that it will favor chiral ordering. Such ordering can accompany conventional magnetic ordering but is sometimes observed even in the absence of magnetic ordering if three or four-spin interaction terms are present [78, 79]. Since we are considering a ladder, we have to be careful about the handedness of the 3 spins used to measure the chirality if we want to have a consistent sign convention. If we label the ith spin on two-legs of the ladder as $\mathbf{S}_{i,1}$ and $\mathbf{S}_{i,2}$ where 1 and 2 refer to the bottom-leg and top-leg, respectively, we can then define the scalar chirality by going around clockwise as follows.

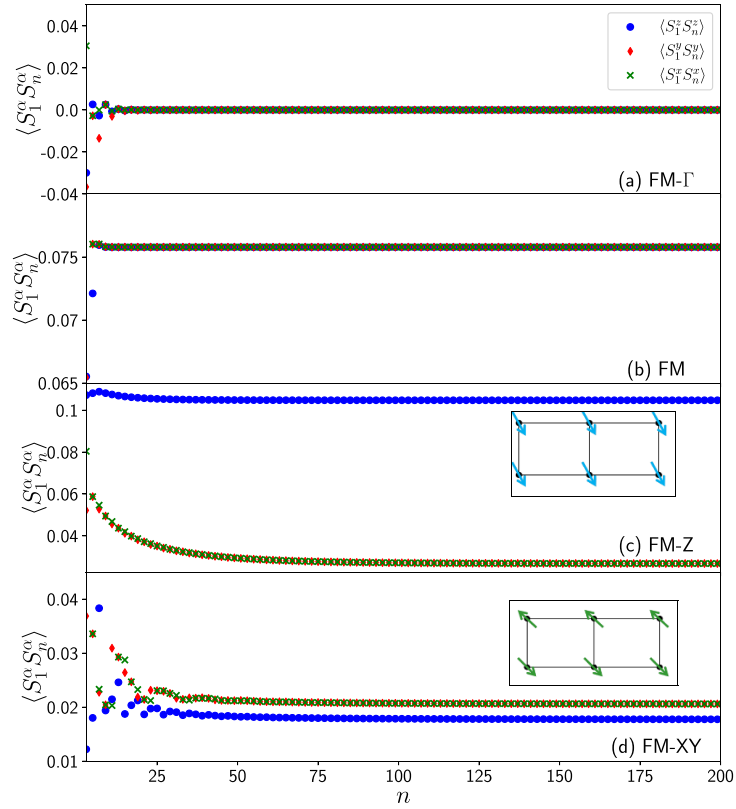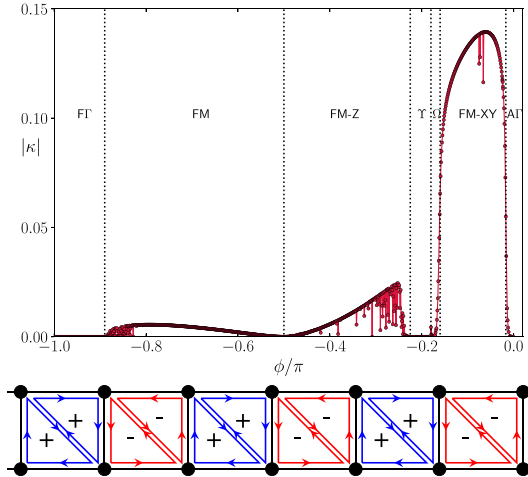$$\kappa = \langle \sigma_{i,1} \cdot (\sigma_{i,2} \times \sigma_{i+1,1}) \rangle. \tag{7}$$

Figure 4. Spin correlation functions $\langle S_1^\alpha S_{1+n}^\alpha \rangle$ as obtained from iDMRG along the lower leg (odd numbered sites) of the ladder starting at $n = 3$ and ending at $n = 199$. Here, n is the site index from figure 1. (a) The FΓ-phase at $\phi/\pi = 0.899$. (b) The FM-phase at $\phi/\pi = 1.299$. (c) The FM-Z-phase at $\phi/\pi = 1.649$. (d) The FM-XY-phase at $\phi/\pi = 1.849$. The insets in panel (c) and (d) are the magnetization $\langle S_i^\alpha \rangle$ in the unit cell, where the horizontal axis is the $+x$ direction and the vertical axis is the $+z$ direction.

Figure 5. Scalar chirality in the FM-XY-phase. Top panel: The scalar chirality $|\kappa|$ versus ϕ/π. Lower panel: An example of the staggered pattern of chirality in the FM-XY-phase at $\phi = 1.9\pi$. Each triangle has $|\kappa| = 0.133$. The scalar chirality in the FM and FM-Z-phases displays an identical staggering, but $|\kappa|$ is an order of magnitude weaker.

We get a consistent sign by always going around clockwise. For example, for the upper triangles where we get $\kappa = \langle \sigma_{i,2} \cdot (\sigma_{i+1,2} \times \sigma_{i+1,1}) \rangle$. For a pictorial representation, if the κ is positive (negative), we assign blue (red) arrows $i \to j \to k$ for $\kappa = \langle \sigma_i \cdot (\sigma_j \times \sigma_k) \rangle$ and all even permutations of i, j, k, with clockwise (anti-clockwise) circulation.

The scalar chirality is non-zero in all three ferromagnetic phases, as can be seen from the top panel of figure 5. It is largest in the FM-XY-phase, where a staggered pattern of chirality is observed, alternating in sign between neighboring plaquettes. A sketch of the staggered pattern is shown in the lower panel of figure 5. At

$\phi = 1.9\pi$ in the FM-XY-phase we find $|\kappa| = 0.133$ with $|\kappa|$ going to zero at the QCP of the FM-XY-phase as shown in the top panel of figure 5. The same staggered pattern of the chirality is also observed in the FM and FM-Z-phases, but the overall magnitude of $|\kappa|$ is about an order of magnitude weaker.

6. AΓ, FΓ and RS-phases

As already discussed briefly in section 2, the points $\phi = 0, \pi/2$ and π within the AΓ, RS and FΓ phases respectively, (see figure 2), have previously been studied for ladder systems. Below, we list the corresponding phases and their associated properties.

- RS-phase: For $\phi/\pi \in (0.380, 0.790)$, we find a RS phase. This follows from the fact that the phase contains the point $\phi = \pi/2$, where $J = 1$ and $\Gamma = 0$, corresponding to the AF Heisenberg ladder. Its ground state is known to be in a disordered rung singlet phase [54, 55], where the spins on each rung of the ladder are coupled into a spin singlet. This can be confirmed by increasing the Heisenberg coupling of the rungs of the ladder, approaching the product state of RSs. The spin correlations for this phase are shown in figure 3(c) and do not show any long-range magnetic ordering as one would expect. The RS-phase is gapped, and it has been classified as a trivial SPT phase [48].

- FΓ-phase: This phase extends over the region $\phi/\pi \in (0.840, 1.110)$ and includes the point $\phi = \pi$ corresponding to the pure ferromagnetic Γ point with $J = 0, \Gamma = -1$. A local unitary transformation, U_6, has been found [44] that maps the ferromagnetic Γ-ladder to a model with AF anisotropic Heisenberg couplings, which is known [41, 42] to be in the same phase as the isotropic AF Heisenberg ladder known to be in the RS-phase. Counterintuitively, the FΓ-phase is then simply related to the RS-phase through the U_6, a phase that is usually associated with AF interactions, and the FΓ-phase is therefore often labelled RS_{U_6}. As to be expected, spin correlations in the FΓ-phase do not show long-range order, as shown in figure 4(a). The FΓ-phase is gapped, with a finite correlation length. Since the FΓ-phase is related to the RS-phase through the local unitary U_6 transformation, the FΓ-phase is also a trivial SPT [48].

- AΓ-phase: This phase extends over only a small region $\phi/\pi \in (1.983, 0.025)$ and the pure AF Γ point at $\phi = 0$, with $J = 0$ and $\Gamma = 1$, has previously been studied in detail [41, 42]. Spin correlations are shown in figure 3(a) show no long-range magnetic order but a characteristic period 3 variation along the leg of the ladder. The phase has a small gap and a sizeable correlation length, with $\xi \sim 41a$ at the pure AF Γ point. The AΓ-phase is a SPT phase protected by TR$\times\mathcal{R}_b$ symmetry, the product of TR and π rotation around the b-axis ($\mathcal{R}_b$) and a string-order parameter has been found [43].

Above, we have briefly discussed the 5 magnetically ordered phases, AF, AF-Z, FM, FM-Z and FM-XY along with the 3 previously known phases, RS, FΓ and AΓ. We now turn to a discussion of the 3 remaining phases, Υ, Ω and δ, all of which show no long-range magnetic order and can be considered as potential SPT phases.

7. Potential new SPT phases

7.1. Correlation length

As is often the case, the most complex part of the phase diagram in figure 2 is the proliferation of phases around the antiferromagnetic Γ-point, with $\phi = \pi$. We therefore study part of this phase diagram in more detail by explicitly calculating the correlation length. For translationally invariant matrix product states (MPS), obtained from iDMRG calculations, the transfer matrix can be defined. For normalized states, the largest eigenvalue of the transfer matrix must be unity, and the second-largest eigenvalue determines the correlation length through the relation $\xi = -N_c/\ln(|\lambda_2|)$. Here, N_c is the number of sites in the unit cell used to define the transfer matrix. For quasi one-dimensional systems, the correlation length is related to the gap, Δ, through the relation $\xi = v/\Delta$ [80], with v a characteristic velocity, expected to be $\mathcal{O}(1)$. If the MPS is obtained with a bond dimension D, the transfer matrix is a $D^2 \times D^2$ matrix, hindering calculations of ξ with a very larger bond dimension. However, a significant advantage is that an estimate of the correlation length can be obtained without explicit calculations of correlation functions.

In figure 6 we show results for the correlation length in the region $\phi/\pi \in [-0.25, 0.1]$ from iDMRG calculations with a bond dimension of $D = 120, 200$ and 300. We first note that ξ shows a divergence at all previously noted QCP. Secondly, all phases shown, FM-Z, Υ, Ω, FM-XY, AΓ, δ and AF, have finite correlation lengths corresponding to a gapped phase. At the mid-point of the potential new SPT phases, we find approximatively $\xi_\Upsilon \sim 21a$ for the Υ-phase, $\xi_\Omega \sim 30a$ for the Ω-phase and $\xi_\delta \sim 57a$ for the δ-phase, with a the lattice spacing. Note that, the spin correlation functions shown in figures 3, 4 and 8 are shown along a single leg of the ladder but versus the site index n from figure 1. As a function of n, they should therefore decay on a length scale that is given by the correlation length in figure 6, obtained from the transfer matrix.
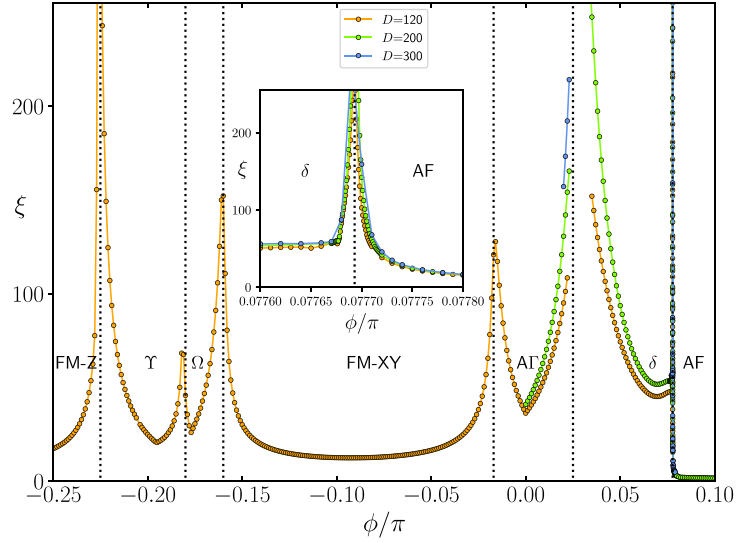
Figure 6. The correlation length, ξ, versus ϕ/π for $\phi/\pi \in [-0.25, 0.1]$ as obtained from the transfer matrix with bond dimension $D = 120\,200\,300$. The inset shows a close up of the δ-AF transition. The dotted lines correspond to the transitions listed in table 1.
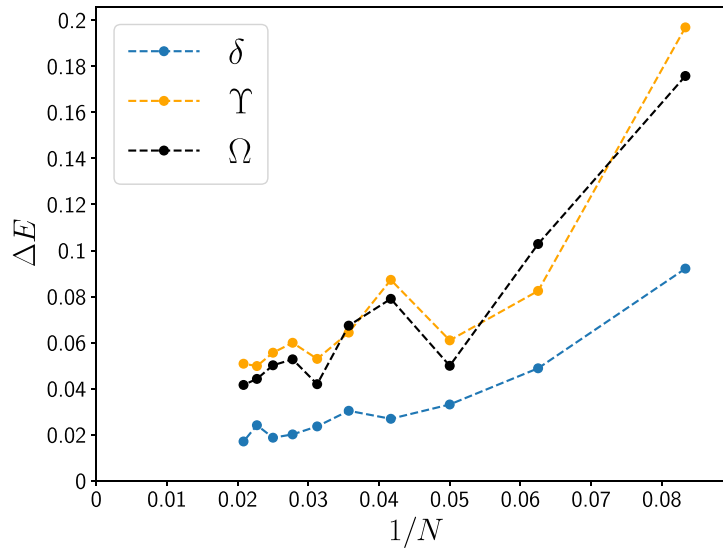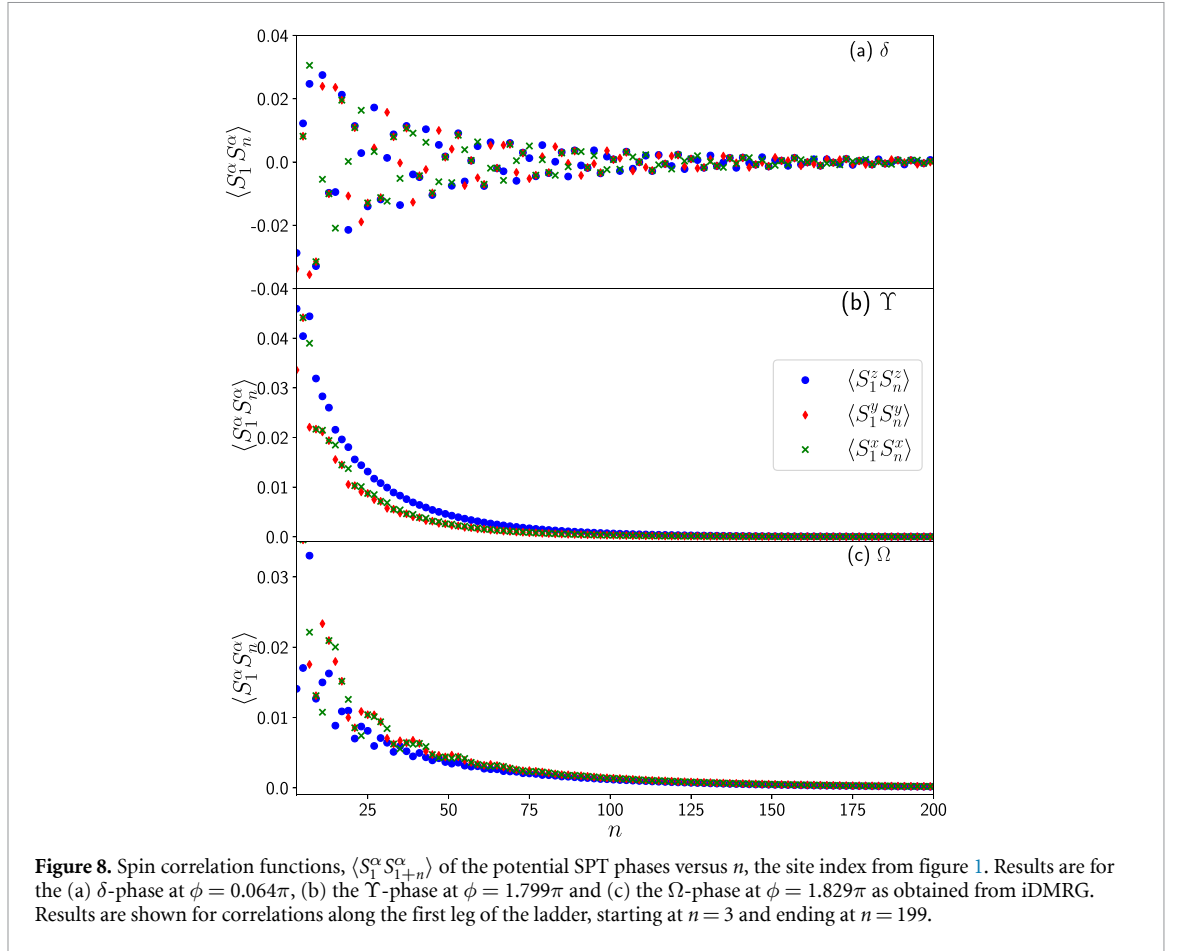

Figure 7. Energy gaps of the δ-phase at $\phi = 0.064\pi$, the Υ-pase at $\phi = 1.799\pi$ and the Ω-phase at $\phi = 1.829\pi$ between the ground state and the first excited state obtained through finite DMRG with a maximal bond dimension $D = 1200$ and periodic boundary conditions. The system sizes shown correspond to $N = 12$ sites to $N = 48$ in increments of 4 sites.

7.2. Spin gap

To confirm the presence of a spin gap in the Υ, Ω and δ phases, we have explicitly evaluated the gap using exact diagonalization on small systems, and finite size DMRG calculations with periodic boundary conditions (PBC) on somewhat larger systems. Our results are shown in figure 7. The dependence on the system size N is not smooth, as one might have expected from the high degree of frustration present in the systems. However, it seems clear that the results for the Υ and δ-phases will converge to a finite small value in the thermodynamic limit, with the gap in the Υ-phase slightly larger than in the Ω-phase. This is consistent with our results for ξ that indicate a smaller ξ in the Υ-phase and therefore likely also a larger gap, when compared to the Ω-phase if the velocities are assumed the same. The results for the δ-phase are more ambiguous, and it seems possible that the gap will tend to zero as $N \to \infty$. However, our results for the ξ in the δ-phase close to the δ-AF transition are very stable and only show a small dependence on the bond dimension D. At $\phi = 0.077\pi$ we have the previously quoted value of $\xi \sim 57a$ obtained with $D = 300$, $\xi \sim 53a$ ($D = 200$) and $\xi \sim 48a$ ($D = 120$). Although these result indicate a sizable correlation length of $\xi \sim 62a$ as $D \to \infty$, the calculations are very stable, excluding the possibility of a correlation length diverging with D

Figure 8. Spin correlation functions, $\langle S_1^\alpha S_{1+n}^\alpha \rangle$ of the potential SPT phases versus n, the site index from figure 1. Results are for the (a) δ-phase at $\phi = 0.064\pi$, (b) the Υ-phase at $\phi = 1.799\pi$ and (c) the Ω-phase at $\phi = 1.829\pi$ as obtained from iDMRG. Results are shown for correlations along the first leg of the ladder, starting at $n = 3$ and ending at $n = 199$.

and lending strong support to the presence of a small but finite gap in the δ-phase. It would be interesting to explore the alternative scenario of a gapless δ phase by studying the spin stiffness [81] in this phase.

7.3. Spin correlation functions

The spin correlation functions for the three phases, Υ, Ω and δ are shown in figure 8 as obtained from iDMRG calculations. While the Υ and Ω-phases show largely ferromagnetic correlations, the δ-phase correlations are intermittently negative, showing a more AF nature. However, in all 3 phases, the spin correlation functions quickly approach zero. No long range magnetic order is observed. As can be seen in figure 5 there are no chiral correlations in the Υ and Ω phases, and we have verified that the same is the case for the δ phase. The three phases therefore appear to have no discernible order, consistent with the phases being gapped SPT phases.

7.4. Projective symmetry analysis of time reversal

While the usual Landau classification of phases do not distinguish between SPT phases, it is possible to develop a classification of such phases based on a projective symmetry analysis [46, 47, 82–85]. This classification takes it starting point in the MPS form of the wave functions for gapped SPT phases where a crucial degeneracy of the entire ES was noted [45, 77].

To proceed, one writes the MPS wavefunction in its canonical form [86–89]:

$$|\Psi\rangle = \sum_{j_1,\ldots,j_N} \Gamma_{j_1}^{[1]} \Lambda^{[2]} \Gamma_{j_2}^{[2]} \ldots \Lambda^{[N]} \Gamma_{j_N}^{[N]} |j_1,\ldots,j_N\rangle, \tag{8}$$

where the $\Gamma_{j_n}^{[n]}$ are complex matrices and the $\Gamma^{[n]}$, real, positive, square diagonal matrices. If we consider infinite systems with translational symmetry from the perspective of iDMRG, the set of matrices on any unit cell becomes the same $\Gamma_j^{[n]} = \Gamma_j$, $\Gamma^{[n]} = \Gamma$ for all n, although they may vary within the unit cell. We now consider a site symmetry operation g. In the spin basis this symmetry operation will be represented by a unitary matrix, $\Sigma_{jj'}(g)$. One can then establish [45, 90] that the Γ_j matrices of bond dimension D, must transform as [45, 76]:
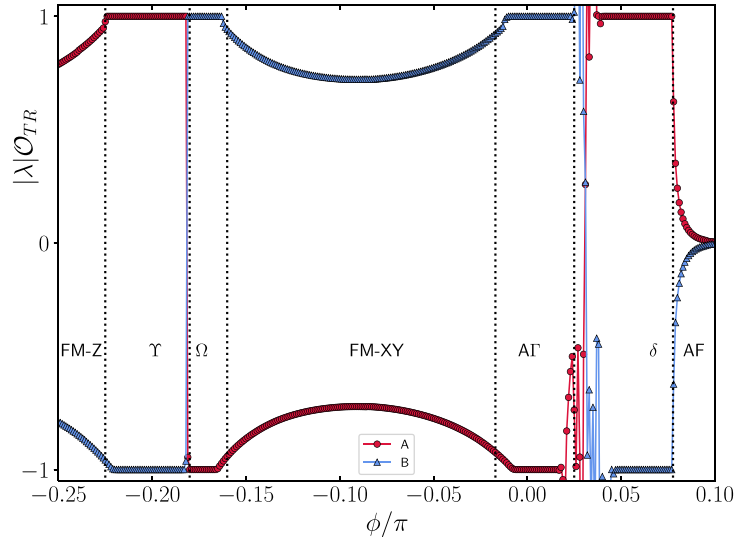
Figure 9. The time-reversal phase factor $|\lambda|\mathcal{O}_{\mathrm{TR}}$ versus ϕ/π as obtained from iDMRG, with $|\lambda|$ the leading eigenvalue of the generalized transfer matrix (10). The red circles correspond to cluster A from figure 1(a) and the blue triangles to cluster B from figure 1(b).

$$\sum_{j'}\Sigma_{jj'}(g)\Gamma_{j'} = e^{i\theta}U^{\dagger}(g)\Gamma_j U(g). \tag{9}$$

Here, $e^{i\theta}$ is a phase factor, and the unitary matrices $U(g)$ commute with the Γ matrices, and form a D-dimensional projective representation of the symmetry group of the wave-function. Exploiting the full machinery of the MPS formulation, one can show that the $U(g)$ matrices be determined from the unique eigenvector of the generalized transfer matrix with eigenvalue $|\lambda| = 1$ [45, 76]. The generalized transfer matrix is here defined as:

$$T^{\Sigma}_{\alpha\alpha';\beta\beta'} = \sum_{j}\left(\sum_{j'}\Sigma_{jj'}\Gamma_{j',\alpha\beta}\right)\left(\Gamma_{j,\alpha'\beta'}\right)^{*}\Lambda_{\beta}\Lambda_{\beta'}, \tag{10}$$

and it is therefore possible to determine the $U(g)$ matrices numerically once the ground-state wavefunction has been determined in a translationally invariant MPS form. The projective representation is reflected in the fact that if $\Sigma(g)\Sigma(h) = \Sigma(gh)$, then

$$U(g)\,U(h) = e^{i\phi(g,h)}U(gh), \tag{11}$$

where the phases $\phi(g,h)$ are characteristic of the topological phase.

For the $J\Gamma$-ladder there are few site symmetries and the ladder does not satisfy D_2 symmetry, nor is it symmetric with respect to interchanging the legs, σ. We therefore focus only on R, defined by $\Gamma_j \rightarrow \sum_{j'}\left[e^{i\pi S^y}\right]_{jj'}\Gamma^{\star}_{j'}$, with $\star$ denoting complex conjugation. In this case, it can be established that [45] $U_{\mathrm{TR}}U^{\star}_{\mathrm{TR}} = e^{i\phi(\mathrm{TR},\mathrm{TR})}\mathbb{1}$ from which it follows that $\phi(\mathrm{TR},\mathrm{TR}) = 0$ or π. If $\phi(\mathrm{TR},\mathrm{TR}) = \pi$ we see that U_{TR} is an antisymmetric matrix and one can then show [45] that this is only possible if all eigenvalues of the ES have even multiplicity, thereby linking the non-trivial value of $e^{i\phi(\mathrm{TR},\mathrm{TR})} = -1$ to the degeneracy of the entanglement spectrum. Furthermore, if the largest eigenvalue of the generalized transfer matrix is smaller than one, $|\lambda| < 1$, then TR is not a good symmetry of the MPS representing the phase.

For time reversal, the phase factor $e^{i\phi(\mathrm{TR},\mathrm{TR})}$ can be extracted by defining [76]:

$$\mathcal{O}_{\mathrm{TR}} \equiv \frac{1}{D}\mathrm{Tr}\left(U_{\mathrm{TR}}U^{\star}_{\mathrm{TR}}\right), \tag{12}$$

with the $D \times D$ matrices U_{TR} extracted numerically from the generalized transfer matrix (10). For instance, for the $S = 1$ spin chain in the Haldane phase, one finds $\mathcal{O}_{\mathrm{TR}} = -1$ [45, 77]. In figure 9 we show results for $|\lambda|\mathcal{O}_{\mathrm{TR}}$ versus ϕ/π for the two different clusters A and B from figure 1. We multiply with $|\lambda|$, the leading eigenvalue of the generalized transfer matrix so that one may immediately see when a phase does not respect the TR symmetry which should be the case for the magnetically ordered phases. This is clearly the case for the FM-Z, FM-XY and AF phases in figure 9 where $|\lambda|\mathcal{O}_{\mathrm{TR}}$ quickly deviates from ± 1. In section 4.1 we

discussed the degeneracy of the ES in the different phases for both cluster A and B. As is clear from figure 9, the non-trivial phase factor $\mathcal{O}_{TR} = -1$ follows the ES degeneracy and jumps between cluster A and B precisely at the QCP. A summary of the results for $\mathcal{O}_{TR}^{A,B}$ for the different phases are included in table 2. Figure 9 shows that if the corresponding cluster is selected, the Υ, Ω, and δ phases all transform non-trivially under TR, as a non-trivial SPT phase. However, we also note that the RS-phase has $\mathcal{O}_{TR}^A = 1$ and $\mathcal{O}_{TR}^B = -1$, and this phase is known to be a trivial SPT phase [48]. For a definite classification of the Υ, Ω, and δ phases as non-trivial SPT phases, a further analysis is therefore needed.

For a more complete picture, it is therefore interesting to study the non-symmorphic symmetry, $\sigma \times \mathrm{tr}(1)$ where σ is the aforementioned operator that interchanges the legs of the ladder while $\mathrm{tr}(1)$ is a translation by 1 lattice spacing in the direction *along* the leg of the ladder. This is a symmetry of the Hamiltonian, equation (1), but, as far as we can tell, not a symmetry of any of the Υ, Ω, and δ phases. Still, these phases could be protected by other symmetries that we have not been able to analyze.

7.5. Uniform field as an active operator

Each of the three phases, Υ, Ω, and δ show a 4-fold degenerate ground-state. It is of considerable interest to determine what perturbations will split the degeneracy between these four states, the so-called active operators [47, 48, 83, 84]. The $J\Gamma$-ladder does not have the usual site symmetries associated with 180° rotation about the $x(y,z)$ axis. However, it does possess the previously mentioned $\sigma \times \mathrm{tr}(1)$ symmetry. To study the active operators, we therefore first consider the behavior of the operator $S_\alpha^T = \sum_i S_i^\alpha$ within the manifold of the 4 ground-states that we label $|1\rangle, |2\rangle, |3\rangle$ and $|4\rangle$. We note that these operators do not break the $\sigma \times \mathrm{tr}(1)$ symmetry. We must have $\langle i|S_\alpha^T|i\rangle = 0$ $\forall i$, since the Υ, Ω, and δ phases are not magnetically ordered. However, $[S_\alpha^T, H] \neq 0$ so we can diagonalize the matrix $\langle i|S_\alpha^T|j\rangle$ and study the eigenvalues. A non-zero s_α indicates that the S_α^T operator is active, splitting the states. In the present case, with $\alpha = x, y, z$, all 4 eigenvalues are sometimes non-zero, which is difficult to interpret. However, given the underlying honeycomb lattice, it is natural to instead study the eigenvalues of S_α^T with $\alpha = a, b, c$, the axis of the honeycomb lattice. Here, a is a unit vector in the $[11\bar{2}]$ direction, b in the $[1\bar{1}0]$ direction and c in the $[111]$ direction. In this case, the results are of the much simpler form $(s_\alpha, -s_\alpha, 0, 0)$, closely resembling what one finds for the $S = 1$ spin chain in the Haldane phase where the 4 ground-states correspond to two free $S = 1/2$ excitations at each end, yielding $(1, -1, 0, 0)$ for $S_{x,y,z}^T$. Results for s_α with $\alpha = a, b, c$ versus system size, N, for the Υ, Ω, and δ phases are shown in figure 10, in each case with cluster A or B from figure 1 yielding the 4 degenerate ground-states. For finite systems, the 4 states are not completely degenerate but split by a small amount, decreasing with N. Some variation with N is therefore to be expected. In addition, given the results from figure 6, showing a large correlation length in all three phases, it is natural to expect that rather large system sizes are needed to see a clear separation of any states localized at the end of the open segments. From studies of the edge excitations in the $S = 1$ chains it is known that these excitations fall off as $\exp(-x/\xi)$ from the end of the chain, with ξ the bulk correlation length [91], extending far into the chain as the borders of the Haldane phase are approached [92]. The clearest results are obtained for the Ω phase, where the results in figure 10(c) show that there is no response to a field in the a and c directions. Furthermore, s_b seems to stabilize around a value $s_b \sim 3$–4, consistent with well-defined edge states. This is the same behavior observed in the AΓ phase which was interpreted as a SPT phase protected by $\mathrm{TR} \times \mathcal{R}_b$ symmetry, the product of TR and π rotation around the b-axis ($\mathcal{R}_b$) [43].

The results for the δ phase, shown in figure 10(a) are more difficult to interpret. With the limited size available, it seems possible that all s_α could attain a finite small value as $N \to \infty$, or s_a and s_c could reach zero with s_b finite, or all could go to zero. The δ phase has the largest correlation length of the three phases, and values of N beyond what we have been able to reach are needed to resolve this.

For the Υ phase, shown in figure 10(b), s_c quickly reach a small finite value $s_c \sim 0.5$, consistent with S_c^T being an active operator. However, surprisingly, s_a and s_b increase with N out to the largest value of N. This is not consistent with S_a^T and S_b^T being active operators. We now turn to a brief description of some specific results for the three potential SPT phases.

7.6. Ω phase

The most promising SPT candidate is the Ω phase, where we have shown that S_b^T is an active operator. It is then interesting to explicit demonstrate the appearance of the edge states by applying a small field term of form $-h_b S_b^T$ to the ladder. However, since the states are not eigenstates of S_b^T, this coupling is not simply a Zeeman term, although for small enough h_b the change in energy should be linear in h_b. Hence, such a linear regime has to be located, and the field carefully applied within the linear regime. We select a field term of $h_b = 10^{-5}$, small enough that for $N = 200$ the change in energy is significantly smaller than the gap in the
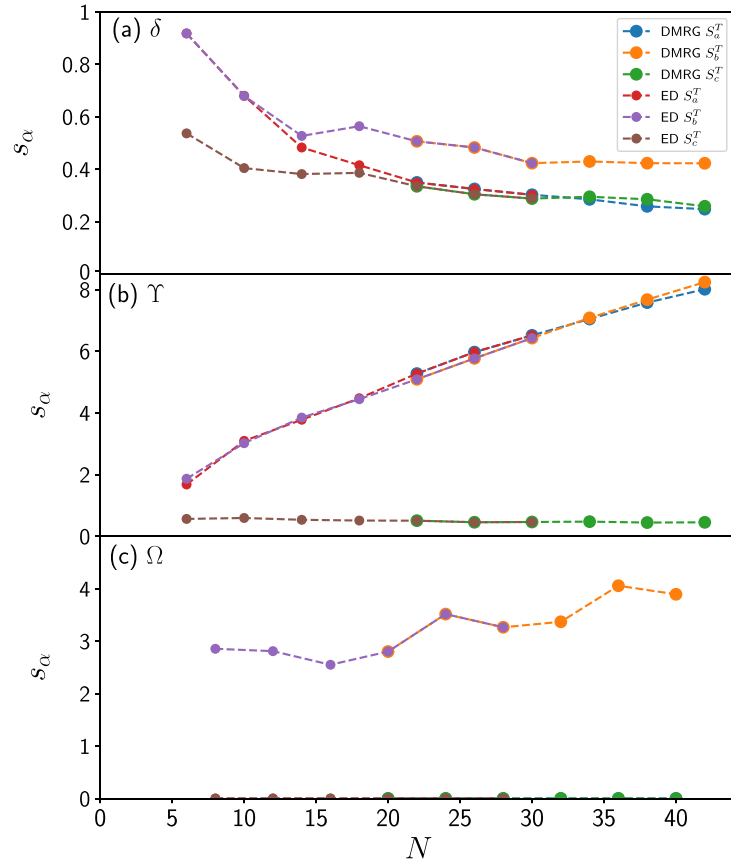
Figure 10. Leading eigenvalue s_α of the total magnetization S_α^T along axis α, with $\alpha = a, b, c$, versus cluster size N. (a) δ-phase at $\phi = 0.064\pi$ with cluster B. (b) Υ-phase at $\phi = 1.799\pi$ with cluster B. (c) Ω-phase at $\phi = 1.829\pi$ with cluster A. For all size until $N = 28$, s is obtained with exact diagonalization (in blue, orange, and green) while the remaining larger sizes are obtained with finite DMRG (red, purple, and brown).

Figure 11. Magnetization $\langle S_n^b \rangle$ from finite DMRG calculations along the $b = [1\bar{1}0]$ direction with a uniform field of $h_b = 10^{-5}$ applied in the b direction at every site. Results are shown for a $N = 200$ ladder in the Ω phase with $\phi = 1.829\pi$. The magnetization on each leg is almost identical.

system. Yet, this field is large enough that the very small finite splitting of the four states is irrelevant. The resulting edge states are shown in figure 11 as obtained from finite DMRG calculations with OBC using cluster A from figure 1. Here n corresponds to the site index, with odd n for the lower leg of the ladder and even n for the upper. Evidently, $\langle S_n^b \rangle$ is the same for both legs. Furthermore, the peak in $\langle S_n^b \rangle$ is not at sites 1, 2 but instead occurs for sites $n = 5, 6$. The decay of the amplitude of $\langle S_n^b \rangle$ is consistent with the previous
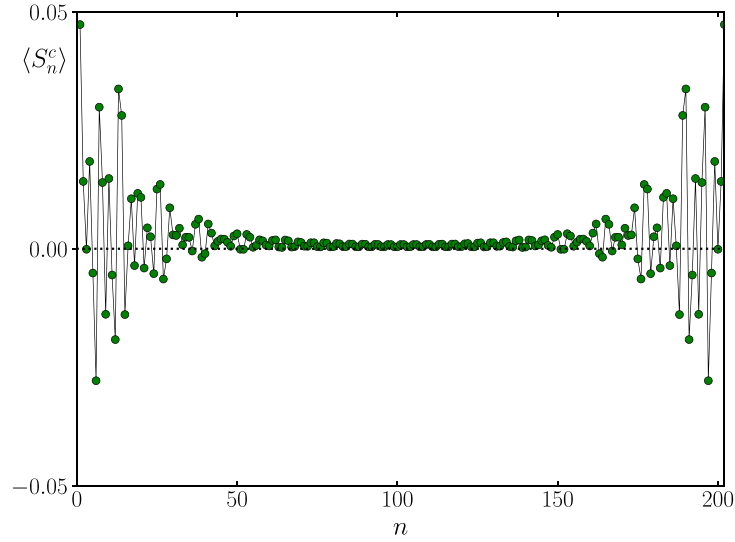
Figure 12. Magnetization $\langle S_n^c \rangle$ from finite DMRG calculations along the $c = [111]$ direction with a uniform field of $|h_c| = 3\times10^{-4}$ applied in the [111] direction at every site. Results are shown for a $N = 202$ ladder on cluster B with OBC, in the Υ phase with $\phi = 1.799\pi$.

estimate of the bulk correlation length of $\xi_\Omega \sim 30a$, and we note that with the small field applied we find $\langle S_b^T \rangle \sim 3$, slightly below the value of 3–4 estimated from the results in figure 10 from much smaller systems with $h_b = 0$.

7.7. Υ phase

In a manner similar to the Ω phase, we can study the edge-states appearing in the Υ phase when the four degenerate ground-states are split by a small field h_c, along the c direction, [111]. We use a field strength of $|h_c| = 3\times10^{-4}$ in the linear regime of the field. The results are shown in figure 12 as obtained from finite DMRG calculations with OBC using cluster B from figure 1. Edge states at either end of the ladder are clearly visible. In contrast to the results for the Ω phase, the two legs of the ladder do not show identical behavior. In fact, due to the shape of cluster B, $\langle S_n^c \rangle$ on the upper leg at the left half of the ladder is identical to the results on the *lower* leg on the right half of the ladder. As expected, the results in figure 12 show $S_c^T \sim 0.52$, consistent with our finding of $s_c \sim 0.5$ in the Υ phase.

7.8. δ phase

For the δ phase, we have not been able to obtain a clear picture of any eventual edge states. One reason for this is likely the very large correlation length, in excess of $\xi_\delta \sim 57a$ throughout the phase. However, another important effect is the appearance of pronounced incommensurate correlations, as we shall now discuss. The first thing we note is that from the results presented in figures 2 and 6, it is clear that the correlation length diverges and the gap goes to zero at either end of the δ phase. The δ phase is then a well-defined phase and not simply a part of either the AΓ or AF phases marked by the onset of incommensurate correlations. We can analyze the correlations by Fourier transforming the $\langle S_i^z S_{i+n}^z \rangle$ correlation functions along the first leg of the ladder. The resulting structure factors $S^{zz}(k)$ are shown in figure 13 for values of ϕ/π starting in the AΓ phase and ending in the AF phase. In the AΓ phase at $\phi = 0$ the correlations along a leg has a simple periodicity of 3, corresponding to a peak in the structure factor at $k = 2/3\pi$. On the other hand, in the AF phase, the peak $S^{zz}(k)$ must be at $k = \pi$. However, inside the δ phase, the peak in $S^{zz}(k)$ moves continuously from $k = 2/3\pi$ to $k = \pi$. Close to the δ-AF transition we show in the inset of figure 13 higher precision results for the behavior of $S^{zz}(k)$. To within our numerical precision, it appears that the peak value of $S^{zz}(k)$ does not jump at the QCP, but indeed moves continuously between the two limits.
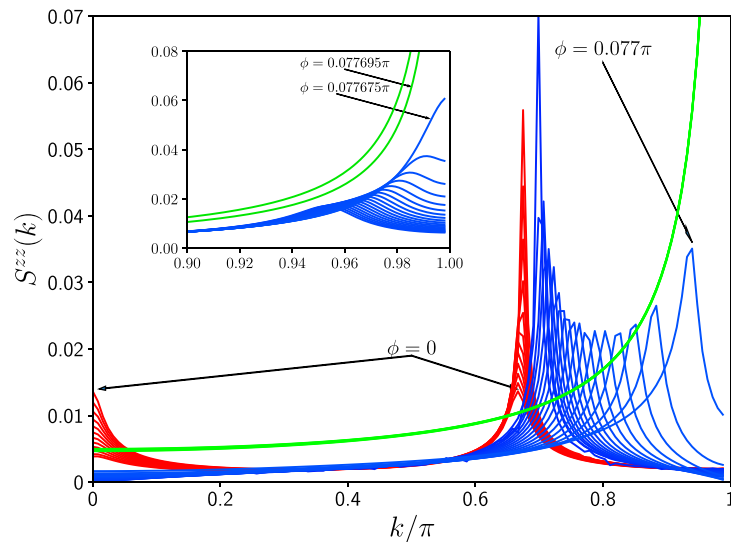
Figure 13. Structure factor $S^{zz}(k)$ from the $\langle S_i^z S_{i+r}^z \rangle$ correlation functions of the AF-Γ, δ and AF phases obtained from iDMRG along the first leg of the ladder, with r is measured along the leg. The red color indicates where $S^{zz}(k)$ is in the AF-Γ phase, transitioning to the δ phase in blue, and ending in the AF phase in green. $S^{zz}(k)$ at $\phi = 0$ is pointed out as having two peaks, one at $k = 0$ and at $k \approx 2/3$. The last point in the δ phase in this sweep is also pointed out at $\phi = 0.077\pi$ before the transition to the AF phase occurs. The inset is a higher precision calculation of $S^{zz}(k)$ near the δ-AF transition. Starting at $\phi = 0.077\,314\pi$ in the δ phase in blue, ϕ is increased to a maximum value of $\phi = 0.077\,716\pi$ in green in the AF phase. The last value in the δ phase occurs at $\phi = 0.077\,675\pi$ while the first value in the AF occurs at $\phi = 0.077\,695\pi$, both centered around $k = 1$.

8. Conclusion

The observation of eleven well-defined phases for the zero field phase diagram of the $J\Gamma$-ladder is remarkable. The proliferation of phases is due to the presence of the Γ interaction term, which lowers the symmetry of the model, allowing for a finely tuned competition between the various phases. It would be of considerable interest to identify low-dimensional materials representative of this model. Presently, we are not aware of any clear candidates. However, the class of Kitaev materials is rapidly expanding, and it is thus plausible that materials with dominant AF Heisenberg interactions and sub dominant Γ-interactions can be found.

Among the eleven phases we have identified three new phases, the Υ, Ω and δ phases which do not show signs of any ordinary long-range magnetic order and could potentially be SPT phases. We have also not found any indication of valence bond ordering. However, we cannot rigorously rule out that the states can be reduced to trivial product states on a large enough length scale. However, such a length scale would have to be sizable, and this scenario seems unlikely. Among the three phases, the Ω phase appears as the most likely SPT phase and clear edge states are observed when a magnetic field is applied along the $[1\bar{1}0]$ direction. Similarly, for the Υ phase, the application of a field along the $[111]$ direction induces clear edge states.

In future work, it would be fascinating to investigate the phase diagram of the $J\Gamma$ ladder in the presence of an applied field, which we expect to show an abundance of new and intriguing phases.

Data availability statement

The data cannot be made publicly available upon publication because they are not available in a format that is sufficiently accessible or reusable by other researchers. The data that support the findings of this study are available upon reasonable request from the authors.

Acknowledgment

ORCID iD

Erik S Sørensen ⬤ https://orcid.org/0000-0002-5956-1190

References

[1] Kitaev A 2006 *Ann. Phys., NY* **321** 2–111
[2] Kugel' K I and Khomskii D I 1972 *JETP Lett.* **15** 446
[3] Kugel' K I and Khomskii D I 1973 *Zh. Eksp. Teor. Fiz.* **64** 429
[4] Kugel' K I and Khomskii D I 1982 *Sov. Phys. - Usp.* **25** 231
[5] Nussinov Z and van den Brink J 2015 *Rev. Mod. Phys.* **87** 1–59
[6] Chaloupka J, Jackeli G and Khaliullin G 2010 *Phys. Rev. Lett.* **105** 027204
[7] Rau J G, Lee E K H and Kee H Y 2016 *Annu. Rev. Condens. Matter Phys.* **7** 195–221
[8] Winter S M, Tsirlin A A, Daghofer M, van den Brink J, Singh Y, Gegenwart P and Valentí R 2017 *J. Phys.: Condens. Matter* **29** 493002
[9] Hermanns M, Kimchi I and Knolle J 2018 *Annu. Rev. Condens. Matter Phys.* **9** 17–33
[10] Takagi H, Takayama T, Jackeli G, Khaliullin G and Nagler S E 2019 *Nat. Rev. Phys.* **1** 264–80
[11] Rousochatzakis I, Perkins N B, Luo Q and Kee H Y 2023 Beyond Kitaev physics in strong spin-orbit coupled magnets (arXiv:2308.01943)
[12] Plumb K W, Clancy J P, Sandilands L J, Shankar V V, Hu Y F, Burch K S, Kee H Y and Kim Y J 2014 *Phys. Rev. B* **90** 041112
[13] Banerjee A *et al* 2016 *Nat. Mater.* **15** 733
[14] Banerjee A *et al* 2018 *npj Quantum Mater.* **3** 8
[15] Janssen L, Andrade E C and Vojta M 2017 *Phys. Rev. B* **96** 064430
[16] Maksimov P A and Chernyshev A L 2020 *Phys. Rev. Res.* **2** 033011
[17] Rau J G, Lee E K H and Kee H Y 2014 *Phys. Rev. Lett.* **112** 077204
[18] Katukuri V M, Nishimoto S, Yushankhai V, Stoyanova A, Kandpal H, Choi S, Coldea R, Rousochatzakis I, Hozoi L and van den Brink J 2014 *New J. Phys.* **16** 013056
[19] Kim H S and Kee H Y 2016 *Phys. Rev. B* **93** 155143
[20] Ran K *et al* 2017 *Phys. Rev. Lett.* **118** 107203
[21] Baek S H, Do S H, Choi K Y, Kwon Y S, Wolter A U B, Nishimoto S, van den Brink J and Büchner B 2017 *Phys. Rev. Lett.* **119** 037201
[22] Kasahara Y *et al* 2018 *Nature* **559** 227–31
[23] Yokoi T *et al* 2021 *Science* **373** 568–72
[24] Lefrançois E *et al* 2022 *Phys. Rev. X* **12** 021025
[25] Bruin J A N, Claus R R, Matsumoto Y, Kurita N, Tanaka H and Takagi H 2022 *Nat. Phys.* **18** 401–5
[26] Czajka P, Gao T A, Hirschberger M, Lampen-Kelley P, Banerjee A, Quirk N, Mandrus D G, Nagler S E and Ong N P 2023 *Nat. Mater.* **22** 36–41
[27] Chern L E, Zhang E Z and Kim Y B 2021 *Phys. Rev. Lett.* **126** 147201
[28] Wang J, Normand B and Liu Z X 2019 *Phys. Rev. Lett.* **123** 197201
[29] Yamada T, Suzuki T and Suga S I 2020 *Phys. Rev. B* **102** 024415
[30] Luo Q, Zhao J, Wang X and Kee H Y 2021 *Phys. Rev. B* **103** 144423
[31] Dagotto E and Rice T M 1996 *Science* **271** 618
[32] Dagotto E 1999 *Rep. Prog. Phys.* **62** 1525
[33] Hickey C and Trebst S 2019 *Nat. Commun.* **10** 530
[34] Gohlke M, Wachtel G, Yamaji Y, Pollmann F and Kim Y B 2018 *Phys. Rev. B* **97** 075126
[35] Gohlke M, Chern L E, Kee H Y and Kim Y B 2020 *Phys. Rev. Res.* **2** 043023
[36] Feng X Y, Zhang G M and Xiang T 2007 *Phys. Rev. Lett.* **98** 087204
[37] Catuneanu A, Sørensen E S and Kee H Y 2019 *Phys. Rev. B* **99** 195112
[38] Agrapidis C E, van den Brink J and Nishimoto S 2018 *Sci. Rep.* **8** 1815
[39] Agrapidis C E, van den Brink J and Nishimoto S 2019 *Phys. Rev. B* **99** 224418
[40] Chaloupka J, Jackeli G and Khaliullin G 2013 *Phys. Rev. Lett.* **110** 097204
[41] Gordon J S, Catuneanu A, Sørensen E S and Kee H Y 2019 *Nat. Commun.* **10** 2470
[42] Sørensen E S, Catuneanu A, Gordon J S and Kee H Y 2021 *Phys. Rev. X* **11** 011013
[43] Sørensen E S and Kee H Y 2023 Twice hidden string order and competing phases in the spin-1/2 Kitaev-Gamma ladder (arXiv:2023.08731)
[44] Chaloupka J and Khaliullin G 2015 *Phys. Rev. B* **92** 024413
[45] Pollmann F, Turner A M, Berg E and Oshikawa M 2010 *Phys. Rev. B* **81** 064439
[46] Chen X, Gu Z C and Wen X G 2011 *Phys. Rev. B* **83** 035107
[47] Chen X, Gu Z C and Wen X G 2011 *Phys. Rev. B* **84** 235128
[48] Liu Z X, Yang Z B, Han Y J, Yi W and Wen X G 2012 *Phys. Rev. B* **86** 195122
[49] Chen J Y and Liu Z X 2015 *Ann. Phys., NY* **362** 551–67
[50] Ueda H and Onoda S 2014 *Phys. Rev. B* **90** 214425
[51] Kariyado T and Hatsugai Y 2015 *Phys. Rev. B* **91** 214410
[52] Ogino T, Furukawa S, Kaneko R, Morita S and Kawashima N 2021 *Phys. Rev. B* **104** 075135
[53] Ogino T, Kaneko R, Morita S and Furukawa S 2022 *Phys. Rev. B* **106** 155106
[54] Dagotto E, Riera J and Scalapino D 1992 *Phys. Rev. B* **45** 5744–7
[55] Barnes T, Dagotto E, Riera J and Swanson E S 1993 *Phys. Rev. B* **47** 3196–203
[56] Luo Q, Zhao J, Kee H Y and Wang X 2021 *npj Quantum Mater.* **6** 57
[57] Rousochatzakis I and Perkins N B 2017 *Phys. Rev. Lett.* **118** 147204
[58] White S R and Noack R M 1992 *Phys. Rev. Lett.* **68** 3487–90
[59] White S R 1992 *Phys. Rev. Lett.* **69** 2863–6
[60] White S R 1993 *Phys. Rev. B* **48** 10345–56
[61] Schollwöck U 2005 *Rev. Mod. Phys.* **77** 259–315
[62] Hallberg K A 2006 *Adv. Phys.* **55** 477–526
[63] Schollwöck U 2011 *Ann. Phys., NY* **326** 96–192 Special Issue
[64] McCulloch I P 2008 Infinite size density matrix renormalization group, revisited (arXiv:0804.2509)
[65] Venuti L C and Zanardi P 2007 *Phys. Rev. Lett.* **99** 095701
[66] Schwandt D, Alet F and Capponi S 2009 *Phys. Rev. Lett.* **103** 170501
[67] Albuquerque A F, Alet F, Sire C and Capponi S 2010 *Phys. Rev. B* **81** 064418

[68] De Chiara G, Lepori L, Lewenstein M and Sanpera A 2012 *Phys. Rev. Lett.* **109** 237208
[69] Lepori L, De Chiara G and Sanpera A 2013 *Phys. Rev.* B **87** 235107
[70] Bayat A, Johannesson H, Bose S and Sodano P 2014 *Nat. Commun.* **5** 3784
[71] Gray J, Bose S and Bayat A 2018 *Phys. Rev.* B **97** 201105
[72] Eisert J and Cramer M 2005 *Phys. Rev.* A **72** 042112
[73] Affleck I, Kennedy T, Lieb E H and Tasaki H 1987 *Phys. Rev. Lett.* **59** 799–802
[74] Affleck I, Kennedy T, Lieb E H and Tasaki H 1988 *Commun. Math. Phys.* **115** 477–528
[75] Kennedy T and Tasaki H 1992 *Phys. Rev.* B **45** 304
[76] Pollmann F and Turner A M 2012 *Phys. Rev.* B **86** 125441
[77] Pollmann F, Berg E, Turner A M and Oshikawa M 2012 *Phys. Rev.* B **85** 075125
[78] Bauer B, Cincio L, Keller B P, Dolfi M, Vidal G, Trebst S and Ludwig A W W 2014 *Nat. Commun.* **5** 5137
[79] Läuchli A, Schmid G and Troyer M 2003 *Phys. Rev.* B **67** 100409
[80] Hastings M B and Koma T 2006 *Commun. Math. Phys.* **265** 781–804
[81] Laflorencie N, Capponi S and Sørensen E S 2001 *Eur. Phys. J.* B **24** 77–84
[82] Gu Z C and Wen X G 2009 *Phys. Rev.* B **80** 155131
[83] Liu Z X, Liu M and Wen X G 2011 *Phys. Rev.* B **84** 075135
[84] Liu Z X, Chen X and Wen X G 2011 *Phys. Rev.* B **84** 195145
[85] Chen X, Gu Z C, Liu Z X and Wen X G 2013 *Phys. Rev.* B **87** 155114
[86] Vidal G 2003 *Phys. Rev. Lett.* **91** 147902
[87] Vidal G 2007 *Phys. Rev. Lett.* **98** 070201
[88] Pérez-García D, Verstraete F, Wolf M M and Cirac J I 2007 *Quantum Inf. Comput.* **7** 401
[89] Orús R and Vidal G 2008 *Phys. Rev.* B **78** 155117
[90] Pérez-García D, Wolf M M, Sanz M, Verstraete F and Cirac J I 2008 *Phys. Rev. Lett.* **100** 167202
[91] Sørensen E S and Affleck I 1994 *Phys. Rev.* B **49** 15771–88
[92] Polizzi E, Mila F and Sørensen E S 1998 *Phys. Rev.* B **58** 2407–10
[93] Fishman M, White S R and Stoudenmire E M 2022 *SciPost Phys. Codebases* 4